

Superradiance in acoustic black hole

Chengye Yu,^{1,*} Xiaolin Zhang,^{1,†} Sobhan Kazempour,^{1,‡} and Sichun Sun^{1,§}

¹*School of Physics, Beijing Institute of Technology, Beijing, 100081, China*

Rotating superradiance in cylinders has recently been observed experimentally using acoustic waves to shed light on the understanding of the superradiant phenomenon in black holes. In this paper, for the first time, we study superradiance in acoustic black holes through theoretical analysis and numerical simulation using COMSOL multiphysics. We find that superradiance can occur in acoustic black holes when the general superradiance condition is met. We also find the amplification effect is significantly weaker in acoustic black holes than in regular cylinders, due to the absorption in such structure.

I. INTRODUCTION

Dicke [1] proposed the concept of superradiant states [2], attributing its amplification to coherence. In 1969, Roger Pense proposed the energy extraction of a rotational black hole as the early version of the superradiance [3, 4]. Later, Zel'Dovich [5, 6] suggests that superradiance can occur on the surface of rotating objects, where the amplitude of the incident wave is significantly larger than the amplitude of the reflected wave. (The phenomenon of superradiance in black holes has also been extensively studied; see [7–26].) Related experiments are then proposed to detect this phenomenon, especially for rotational superradiance [2, 27–31]. In experiments, rotational superradiance occurs when an object moves around a rotational axis with a specific angular velocity, and the condition for superradiance is

$$\omega - m\Omega < 0, \quad (1)$$

, where ω is the incident waves' frequency, m , is the azimuthal quantum number with respect to the axis of rotation, and Ω is the angular frequency of the cylinder. Eq. (1) represents the most general condition for superradiance, and it serves as an indicator for determining whether the phenomenon of superradiance occurs [32–36].

It is found that low-frequency sound modes with orbital angular momentum (OAM) [37, 38] are transmitted through an absorbing rotating disk and amplified when the disk rotation rate meets superradiant conditions [39, 40]. This rotational Doppler effect [41, 42] has also been observed in light-carrying OAM that is backscattered from a rotating rough surface, enabling the remote measurement of an object's rotation speed [43–45]. There are other methods to detect superradiance; for example, Teukolsky et al [46] proposed the idea of creating a "perfect mirror" in a so-called black hole bomb [47, 48]. Numerical studies of charged black hole

bombs at the linear level in the field amplitude have been conducted in both the frequency and time domains, as in Refs. [15, 49, 50], while analytical studies have been carried out in Refs. [51, 52].

Despite the significant progress made in the study of superradiance, there is still a lack of understanding of the phenomenon in certain systems, such as acoustic 'black hole' (ABH). ABHs are systems that mimic the behavior of black holes in general relativity but in the context of acoustic waves [53]. The concept of ABH is derived from the gravitational effects of astronomical black holes [54]. As widely known, the information that approaches a black hole is absorbed and debatably transmitted outside the black hole in the form of Hawking radiation [55–59]. In engineering, researchers discovered that by altering the surface structure of a solid, the elastic wave propagating within it can be absorbed by a wedge structure, creating an effect analogous to the gravitational pull of a black hole. This phenomenon is referred to as ABH structure [60–64]. The study of superradiance in ABHs is important because it can provide insights into the behavior of black holes and the emission of radiation from rotating systems.

The paper is organized as follows: In Section II, we introduce the ABH and derive the amplification factor of the ABH by solving the radial equation with the relevant boundary conditions. In Section III, we utilize semi-analytical and simulation using COMSOL multiphysics software [65–67] to validate superradiance conditions and amplification factors. Finally, in Section IV, we summarize our main results and discuss the implications of our findings.

II. ACOUSTIC BLACK HOLE SET-UP

The physical structure of two-dimensional ABH is given by [61]. The plate consists of a section with a constant thickness h_2 extending from R to the edge of the plate, a tapered region (from r_1 to R), and a central plateau from 0 to r_1 with a constant thickness h_1 . The shape is as below:

$$h(r) = \begin{cases} h_2 & (r \geq R), \\ a(r - r_1)^n + h_1 & (r \leq R). \end{cases} \quad (2)$$

* chengyeyu1@hotmail.com

† xiaolinzhang66@outlook.com

‡ sobhan.kazempour1989@gmail.com

§ sichunssun@gmail.com

The extreme case with $h_1 = r_1 = 0$ and $n \geq 2$ corresponds to an ideal ABH structure (see Fig. 1). In this paper, we set the following parameters for ABH structure: $a = 7.34 \times 10^{-4} m^{-1}$, $r_1 = 2 \times 10^{-2} m$, $h_1 = 6 \times 10^{-4} m$ and $n = 2$ (correspond to the **Simulation analysis** in Sec. IV), and the superradiance analytical analysis in ABH is derived in Sec. III.

III. SUPERRADIANCE MODE

We start from Kirchhoff's equation [68] for a quiescent inviscid and non-conducting fluid, with the equation of mass conservation $\partial\rho/\partial t + \nabla\rho\boldsymbol{\nu} = 0$ and the momentum conservation $\rho\partial\boldsymbol{\nu}/\partial t = -\nabla p$. In the air ($r > R$) we have

$$\begin{aligned} i\omega\rho_+ + \rho_0\nabla\boldsymbol{\nu}_+ &= 0, \\ i\omega\rho_0\boldsymbol{\nu}_+ + \nabla p_+ &= 0, \\ p_+ &= c_s^2\rho_+, \end{aligned} \quad (3)$$

while the ABH is described by the model ($r < R$)

$$\begin{aligned} i\omega\rho_- + \rho_f\nabla\boldsymbol{\nu}_- &= 0, \\ i\omega\rho_f\boldsymbol{\nu}_- + \nabla p_- &= 0, \\ p_- &= c_{eff}^2\rho_-, \end{aligned} \quad (4)$$

where R is the radius of ABH. Zel'dovich's original "dynamical" argument [5, 6] follows the Lorentz-invariant Klein-Gordon equation, and through Eq. (3), we have $\square p_+ = 0$ outside the ABH.

In a coordinate system where the medium is at rest, the absorption can be characterized by a parameter α , causing Eq. (4) to become a modified equation

$$\square p_- = \frac{\alpha}{c_{eff}^2} \partial_t p_- \quad (5)$$

We reconsider the wave equation (3) outside the ABH in cylindrical coordinates, and the radial equation reduces exactly to

$$\frac{1}{r} \frac{\partial}{\partial r} \left(r \frac{\partial p_+(r)}{\partial r} \right) + \left[\frac{\omega^2}{c_s^2} - \frac{m^2}{r^2} \right] p_+(r) = 0. \quad (6)$$

Dissipation is essential for the generation of the superradiance. In the rotating coordinate system, $\alpha(\omega - m\Omega)$ replaces $\alpha\omega$ under the superradiation condition, meaning that the absorption term becomes an amplification term, allowing superradiance to occur [2]. Inside the ABH, the wave equation (5) can be rewritten in the more convenient form

$$\frac{1}{r} \frac{\partial}{\partial r} \left(r \frac{\partial p_-(r)}{\partial r} \right) + \left[\frac{\kappa^2}{c_{eff}^2(r)} - \frac{m^2}{r^2} \right] p_-(r) = 0, \quad (7)$$

where

$$\kappa = \sqrt{\omega^2 + i\alpha(\omega - m\Omega)}, \quad c_{eff}(r) = \sqrt{c_s^2 - v^2(r)}, \quad (8)$$

where κ is the complex angular frequency. The ABH contains an effective complex sound velocity $c_{eff}(r)$ (where c_s is the sound speed) relative to the radial distance r , with $v(r)$ representing the background flow rate[69]. The solution to Eq. (6) is the combination of Bessel functions,

$$p_+(r) = C_1 J_m(\omega r/c_s) + C_2 Y_m(\omega r/c_s), \quad (9)$$

where the coefficient C_1 and C_2 are related to the incident (reflected) part with amplitude for outside ABH. It is worth noting that ω/c_s is the number of sound waves outside ABH. It is evident that the solution to Eq. (7) depends on the background flow rate $v(r)$. Notably, whether the background flow rate is constant or not significantly influences the internal solutions of the ABH. Therefore, this aspect will be the focus of discussion in the next section.

Before working out explicitly the case of a rotating object in (r, φ, z) spatial coordinates with a dissipative surface at $r = R$, we need consider a small quantity ε relative to R that outside surface R_+ is $R + \varepsilon$ and inside surface R_- is $R - \varepsilon$. Obviously, in Fig. 2, a discontinuity exists between the outer surface R_+ and the inner surface R_- , requiring continuity conditions to ensure smoothness on the scattering surface. We consider matching the pressure and velocity of the internal and external solutions under the jump condition of $r = R$ [70]. From the continuity of velocity ($\boldsymbol{\nu}_+ = \boldsymbol{\nu}_-$) in Eqs. (3), (4), we can get

$$\frac{\partial p_+(r)}{\partial r} \Big|_{r=R_+} = \frac{\rho_0}{\rho_f} \frac{\partial p_-(r)}{\partial r} \Big|_{r=R_-}. \quad (10)$$

We can define the impedance inside and outside the ABH and they are different. Since sound scattering occurs at the boundary of the ABH, we assume the small quantity is negligible, allowing us to obtain the associated impedance as

$$Z_+ = \rho_0 c_s, \quad Z_- = \rho_f c_{eff}(r) \Big|_{r=R_-} = \rho_0 c_s Z, \quad (11)$$

where Z_+ is the outside impedance, Z_- is the inside impedance, and Z is the characteristic acoustic impedance of the fibrous material[71] (see Fig. 2).

Due to the mismatch in acoustic impedance between the external and internal environments, the incident wave encounters inside impedance conditions at the scattering interface $r = R$. In terms of impedance, the boundary condition for both sound and surface waves in the rest frame of ABH is

$$p_+(R_+) - p_-(R_-) = -\frac{Z_-}{i\rho_0\omega} \frac{\partial p_+(r)}{\partial r} \Big|_{r=R_+}. \quad (12)$$

When the object rotates uniformly with angular velocity Ω , it is sufficient to transform to a new angular coordinate $\tilde{\phi} = \phi + \Omega t$, which effectively amounts to the replacement of ω with $\omega - m\Omega$ in Eq. (12). Then the inside impedance condition (12) becomes

$$p_+(R_+) - p_-(R_-) = -\frac{Z_-}{i\rho_0(\omega - m\Omega)} \frac{\partial p_+(r)}{\partial r} \Big|_{r=R_+}. \quad (13)$$

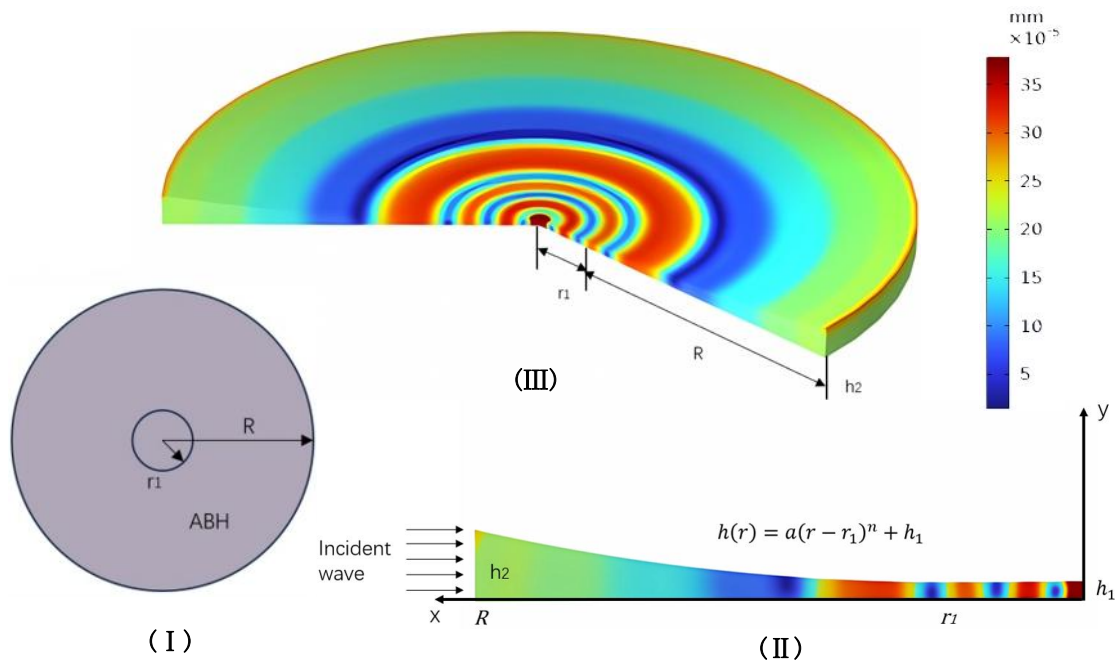


FIG. 1. (I) Sketch of a top view of ABH. (II) A slice view of two-dimensional ABH simulated by COMSOL. (III) 3D view of ABH. Color scheme: Range of displacement induced by a $1Pa$ point load applied at the boundary of the ABH, where the simulation is transient and the azimuthal mode number $m = 0$.

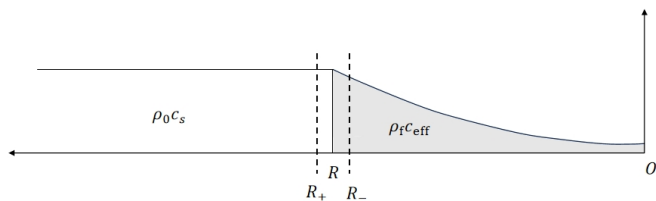


FIG. 2. Outside impedance and inside impedance of the ABH.

Then through Eq. (10), (13), the relationship between coefficients C_1 and C_2 is

$$\frac{C_1}{C_2} = -\frac{\tilde{Z}Y'_m(\omega R_+/c_s) - Y_m(\omega R_+/c_s)}{\tilde{Z}J'_m(\omega R_+/c_s) - J_m(\omega R_+/c_s)}, \quad (14)$$

where

$$\tilde{Z} = Z\left(\frac{\omega}{c_{eff}(r)} \frac{p_-(r)}{\partial_r p_-(r)} \Big|_{r=R_-} - \frac{\omega}{i(\omega - m\Omega)}\right), \quad (15)$$

where $'$ means derivative with respect to the argument. The relationship between the reflected (incident) part with amplitude and coefficients C_1 , C_2 is $C_1 - iC_2$ ($C_1 + iC_2$). For simplicity, letting $C = C_1/C_2$, and amplification factor can be written as

$$\rho = \left| \frac{C - i}{C + i} \right|^2 - 1. \quad (16)$$

One of the conditions for rotational superradiance is $\omega - m\Omega$, where the superradiant phenomenon occurs on the radiating surface of the cylinder, that is, $\rho > 0$. It is worth mentioning that if the cylinder is conventional and not ABH inside, then the amplification factor (16) is different, which we will discuss more in the section IV.

IV. SEMI-ANALYTICAL AND SIMULATION ANALYSIS

In this section, we perform semi-analytical and COMSOL simulations to study the superradiance relation of the sound wave angular frequency and cylinder/ABH angular velocity. The two methods obtain amplification factors for a cylinder and ABH, respectively, and agree well. First of all, we give a brief introduction to the analysis methods to ensure the consistency of the theoretical and simulation analysis.

Semi-analytical analysis: We use Eq. (16) to calculate amplification factor, for semi-analytical calculation

Simulation analysis: In this paper, COMSOL software is used to simulate the acoustic superradiant phenomenon occurring in a fluid domain, and the amplification factor ρ_s of the cylinder or ABH is obtained by setting appropriate boundary conditions with the pressure acoustic module and Delany-Bazley-Miki model [71, 72]. The amplification factor ρ_s is the ratio between the back-

ground sound pressure level and the scattered sound pressure level.

Settings: The values of the parameter in Eq. (16) are fixed as: the density of air is $1.2kg/m^3$, the sound speed of air c_s is $343m/s$, the radius of the cylinder R is $10^{-1}m$ and the azimuthal quantum number is $m = 1$. The value of sound absorption parameter α does not impact much on the superradiant intensity. For simplicity we set $\alpha = 0s^{-1}$. Other parameters are mentioned in section II.

When the background fluid rate $v(r)$ is constant, Eq. (7) is just the inner solution of the cylinder, and its solution can also be expressed as the Bessel function

$$p_-(r) = C_3 J_m(\kappa r / c_{eff}), \quad (17)$$

When the background fluid rate changes, if we assume that the rate $v(r)$ changes gently with radial r , then approximated by WKB, the internal solution of the ABH is

$$p_-(r) \sim \frac{1}{\sqrt{r c_{eff}(r)}} \exp(i \int \frac{\kappa}{c_{eff}(r)} dr). \quad (18)$$

The characteristic acoustic impedance of the fiber material is

$$Z = 1 + A_1 X^{-A_2} - i A_3 X^{-A_4}, \quad X = \rho_0 \omega / \varpi, \quad (19)$$

where ϖ is the flow resistance of the material, ρ_0 is the air density. For the small frequency that $X \leq 0.025$, we can use the values below. We mainly examine glass fiber and rock materials, with their specific acoustic impedance parameters shown in Table I.

TABLE I. Characteristic acoustic impedance for low-frequency Glass (Rock) fiber.

Materials[73]	X	A_1	A_2	A_3	A_4
Low Glass fibre(LG) ≤ 0.025	0.0688	0.707	0.196	0.549	
Low Rock fibre(LR) ≤ 0.025	0.081	0.699	0.191	0.556	

TABLE II. The different values of flow resistances we used in the plot.

Flow resistance (ϖ)	ϖ_1	ϖ_2	ϖ_3
Value ($Pa \cdot s/m^2$)	$1 * 10^4$	$2 * 10^4$	$5 * 10^4$

It is worth mentioning that two conditions are essential: the first is the impedance of the fibrous material attenuation term Z , and the second is the superradiant condition $\omega - m\Omega < 0$, which determines whether the superradiance can occur.

A. Simulation of acoustic superradiance in a fluid domain

1. Sound field ABH in the non-rotational case

This section investigates the sound field distribution of ABHs in a fluid domain. Firstly we analyze the sound

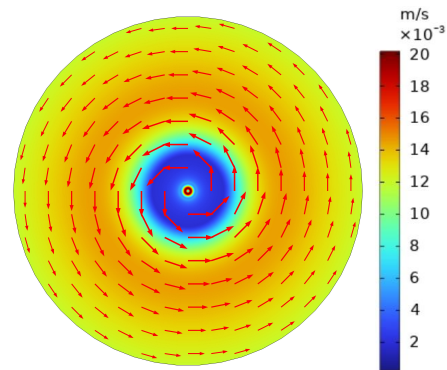


FIG. 3. The distribution of a sound field in an ABH where the frequency of the sound wave is $100Hz$ and the angular velocity of the ABH is $0rad/s$. Color scheme: Range of transient sound speed induced by the specified acoustic pressure field

field distribution in a static fluid domain before extending the study to a rotating fluid domain.

Fig. 3 illustrates the distribution of sound waves with an azimuth mode $m = 1$ within an ABH in a quiescent flow field. The fluid flow field has both the angular and radial velocity components characterized by the azimuthal number m . The effect of the acoustic black hole is that the sound speed decreases towards the singularity. Notice the artifact we put in by hand near the center plateau region in this simulation.

2. Rotational Superradiance

The key to acoustic superradiation is the superradiation condition, where the relation of the angular frequency ω and rotational frequency Ω enables superradiation amplification. In this section, the angular velocity of the acoustic black hole is set to be $200\pi rad/s$ with different incident sound wave frequencies.

Fig. 4 illustrates the non-superradiation case. In this case, the sound waves tend to converge at the black hole's 'event horizon' rather than its 'singularity', dividing the sound field into three regions: the outer high-velocity region (near the 'event horizon'), the middle medium-velocity region, and the inner low-velocity region (near the 'singularity'). We can see the radial rotational effect in this plot compared to the static Fig.3.

Fig. 5 satisfies the superradiation condition, and it has instability in the fluid domain. In the radial direction, the sound wave propagates outward in some region, effectively indicating that the superradiation condition $\omega - m\Omega$ replaces the inherent angular frequency ω of the sound wave. This observation is critical in detecting the amplification effect of acoustic superradiation and provides a foundation for future experimental observations of superradiation phenomena.

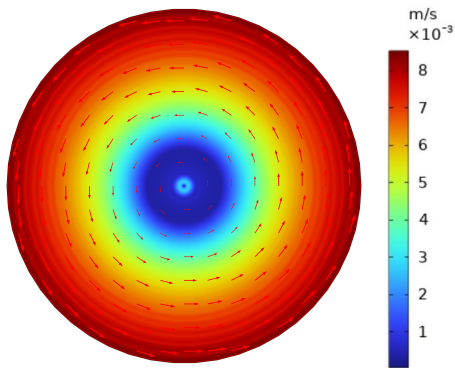


FIG. 4. The distribution of a sound field in an ABH where the frequency of the sound wave is 200Hz , and the angular velocity of the ABH is $200\pi\text{rad/s}$. Color scheme: range of transient sound speed induced by the specified acoustic pressure and the rotation.

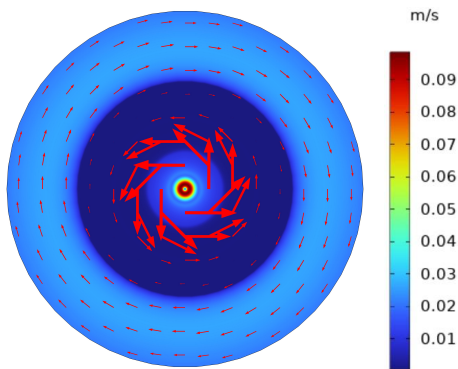


FIG. 5. The distribution of a sound field in an ABH where the frequency of the sound wave is 20Hz , and the angular velocity of the ABH is $200\pi\text{rad/s}$. The propagation direction of sound waves is in the radial direction of the ABH. Color scheme: Range of transient sound speed induced by the specified acoustic pressure field and the rotation.

B. Superradiance for ABH

Unlike the amplification factor ρ of the semi-analytical analysis, the amplification factor of the COMSOL simulation can be written as

$$\rho_s = \frac{L_{p,s}}{L_{p,b}} - 1, \quad (20)$$

where $L_{p,s}$ is the scattering sound pressure level and $L_{p,b}$

is the background sound pressure level. In the simulation, with an incident wave amplitude of 1Pa in air, the background sound pressure level $L_{p,b}$ is measured as 90.969dB .

Fig. 6 shows that when the impedance Z changes with increasing flow resistance of the fiber material, the amplification factor decreases. This suggests that the properties of the fiber material have a significant impact on the superradiant phenomenon. It also suggests when the flow resistance of the fiber material becomes sufficiently large, the observation of superradiance can be considerably challenging.

Unlike a regular cylinder, ABH exhibits a strong absorption effect, causing the sound waves largely trapped within ABH. This phenomenon is clearly illustrated in Fig. 6, and the ABH internal structure causes the absorption of sound waves in simulation. For a regular cylinder, the amplification factors is similar to the results of V. Cardoso et al[2, 28].

V. CONCLUSION

In conclusion, our analysis has provided a first understanding of the superradiant mode in ABHs. By examining the radial equations of ABH both inside and outside the boundary, we derive the superradiant mode formulas. Our results reveal that the internal structure of ABH significantly weakens the superradiant amplification compared to a regular cylinder due to the sound absorption properties of ABH. In addition, the relation between sound wave frequency and angular velocity is studied in simulation, and the generation process of superradiation mode in acoustic black holes is shown. This study also shows the importance of the properties of the fiber material in generating the superradiant mode and further research is needed to fully understand different materials. Our study has important implications for the superradiant experiments. Hopefully, we can observe the superradiant phenomenon by selecting appropriate acoustic materials and optimizing experimental conditions. In summary, the combination of semi-analytical and simulation methods has allowed us to have a deeper understanding of the superradiant phenomenon in ABHs and its comparison with a regular cylinder. Our results have important implications for the detection of the superradiant effect in experiments and provide valuable guidance for future research in this area.

-
- [1] R. H. Dicke, *Phys. Rev.* **93**, 99 (1954).
 [2] R. Brito, V. Cardoso, and P. Pani, *Superradiance*, Vol. 906 (2015).
 [3] R. Penrose, *Nuovo Cimento Rivista Serie* **1**, 252 (1969).
 [4] R. Penrose, *Gen. Relativity Gravitation* **34**, 1141 (2002).
 [5] Y. B. Zel'Dovich, *JETP* **35**, 1085 (1972).

- [6] Y. B. Zel'Dovich, *JETP Letters* **14**, 180 (1971).
 [7] S. Hod, *Phys. Lett. B* **758**, 181 (2016), [arXiv:1606.02306 \[gr-qc\]](https://arxiv.org/abs/1606.02306).
 [8] A. Arvanitaki, S. Dimopoulos, S. Dubovsky, N. Kaloper, and J. March-Russell, *Phys. Rev. D* **81**, 123530 (2010), [arXiv:0905.4720 \[hep-th\]](https://arxiv.org/abs/0905.4720).

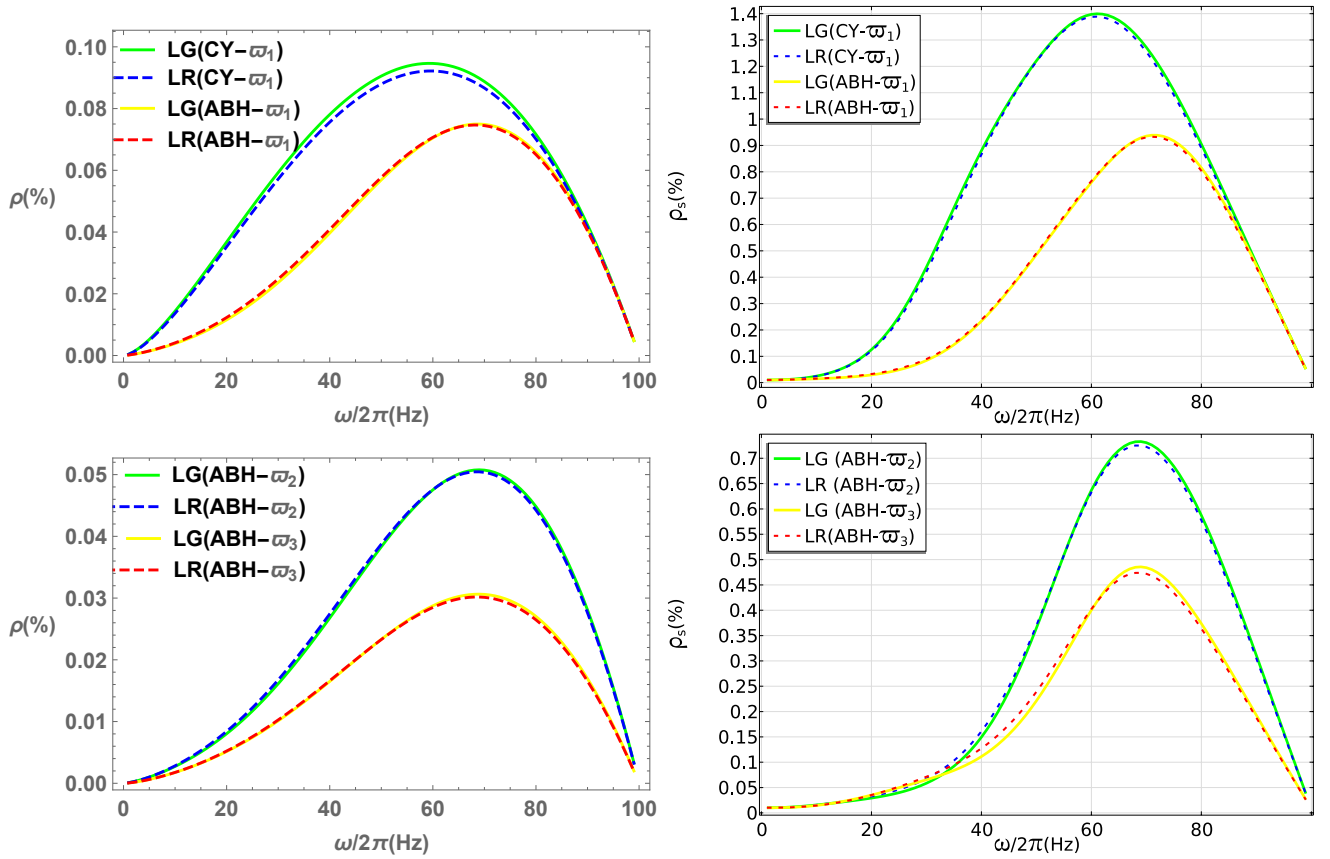


FIG. 6. The left figures show the amplification factor ρ under semi-analytical analysis, and the right figures show the amplification factor ρ_s under simulation. CY stands for cylindrical structure and ABH stands for ABH structure.

- [9] A. Arvanitaki and S. Dubovsky, *Phys. Rev. D* **83**, 044026 (2011), [arXiv:1004.3558 \[hep-th\]](#).
- [10] N. Andersson and K. Glampedakis, *Phys. Rev. Lett.* **84**, 4537 (2000), [arXiv:gr-qc/9909050 \[gr-qc\]](#).
- [11] V. Cardoso and Ó. J. Dias, *Phys. Rev. D* **70**, 084011 (2004), [arXiv:hep-th/0405006 \[astro-ph\]](#).
- [12] H. Witek, V. Cardoso, A. Ishibashi, and U. Sperhake, *Phys. Rev. D* **87**, 043513 (2013), [arXiv:1212.0551 \[gr-qc\]](#).
- [13] V. M. Mehta, M. Demirtas, C. Long, D. J. E. Marsh, L. McAllister, and M. J. Stott, *JCAP* **2021**, 033 (2021), [arXiv:2103.06812 \[hep-th\]](#).
- [14] M. Baryakhtar, R. Lasenby, and M. Teo, *Phys. Rev. D* **96**, 035019 (2017), [arXiv:1704.05081 \[hep-ph\]](#).
- [15] J. C. Degollado, C. A. R. Herdeiro, and H. F. Rúnarsson, *Phys. Rev. D* **88**, 063003 (2013).
- [16] J. C. Degollado, C. A. R. Herdeiro, and E. Radu, *Phys. Lett. B* **781**, 651 (2018), [arXiv:1802.07266 \[gr-qc\]](#).
- [17] R. Brito, V. Cardoso, and P. Pani, *Class. Quantum Grav.* **32**, 134001 (2015), [arXiv:1411.0686 \[gr-qc\]](#).
- [18] S. Ghosh, E. Berti, R. Brito, and M. Richartz, *Phys. Rev. D* **99**, 104030 (2019), [arXiv:1812.01620 \[gr-qc\]](#).
- [19] M. Casals, S. Dolan, P. Kanti, and E. Winstanley, *JHEP* **2008**, 071 (2008), [arXiv:0801.4910 \[hep-th\]](#).
- [20] J. G. Rosa and T. W. Kephart, *Phys. Rev. Lett.* **120**, 231102 (2018), [arXiv:1709.06581 \[gr-qc\]](#).
- [21] W. E. East and F. Pretorius, *Phys. Rev. Lett.* **119**, 041101 (2017), [arXiv:1704.04791 \[gr-qc\]](#).
- [22] R. A. Konoplya and A. Zhidenko, *JCAP* **2016**, 043 (2016), [arXiv:1606.00517 \[gr-qc\]](#).
- [23] M. Richartz, A. Prain, S. Liberati, and S. Weinfurtner, *Phys. Rev. D* **91**, 124018 (2015), [arXiv:1411.1662 \[gr-qc\]](#).
- [24] M. Wang and C. Herdeiro, *Phys. Rev. D* **93**, 064066 (2016), [arXiv:1512.02262 \[gr-qc\]](#).
- [25] H. Yoshino and H. Kodama, *PTEP* **2014**, 043E02 (2014), [arXiv:1312.2326 \[gr-qc\]](#).
- [26] C.-Y. Zhang, S.-J. Zhang, P.-C. Li, and M. Guo, *JHEP* **2020**, 105 (2020), [arXiv:2004.03141 \[gr-qc\]](#).
- [27] S. Endlich and R. Penco, *JHEP* **2017**, 52 (2017), [arXiv:1609.06723 \[hep-th\]](#).
- [28] V. Cardoso, A. Coutant, M. Richartz, and S. Weinfurtner, *Phys. Rev. Lett.* **117**, 271101 (2016), [arXiv:1607.01378 \[gr-qc\]](#).
- [29] J. D. Bekenstein and M. Schiffer, *Phys. Rev. D* **58**, 064014 (1998), [arXiv:gr-qc/9803033 \[gr-qc\]](#).
- [30] D. Faccio and E. M. Wright, *Phys. Rev. Lett.* **123**, 044301 (2019).
- [31] T. Torres, S. Patrick, A. Coutant, M. Richartz, E. W. Tedford, and S. Weinfurtner, *Nat. Phys.* **13**, 833 (2017).
- [32] V. L. Ginzburg and I. M. Frank, *J. Phys. (USSR)* **9**, 353 (1945).
- [33] P. M. Saffin, Q.-X. Xie, and S.-Y. Zhou, *Phys. Rev. Lett.* **131**, 111601 (2023), [arXiv:2212.03269 \[hep-th\]](#).
- [34] D. Yang, S.-h. Oh, J. Han, G. Son, J. Kim, J. Kim, M. Lee, and K. An, *Nature Photon.* **15**, 272 (2021), [arXiv:1906.06477 \[quant-ph\]](#).

- [35] J. Kim, S.-h. Oh, D. Yang, J. Kim, M. Lee, and K. An, *Nature Photon.* **16**, 707 (2022), arXiv:2406.15710 [quant-ph].
- [36] M. Jeon, J. Kim, and K. An, (2024), arXiv:2408.09486 [quant-ph].
- [37] J. F. Nye and M. V. Berry, *Proc. R. Soc. Lond. A* **336**, 165 (1974).
- [38] K. Volke-Sepúlveda, A. O. Santillán, and R. R. Boullosa, *Phys. Rev. Lett.* **100**, 024302 (2008).
- [39] M. Cromb, G. M. Gibson, E. Toninelli, M. J. Padgett, E. M. Wright, and D. Faccio, *Nat. Phys.* **16**, 1069 (2020), arXiv:2005.03760 [physics.class-ph].
- [40] G. M. Gibson, E. Toninelli, S. A. R. Horsley, G. C. Spalding, E. Hendry, D. B. Phillips, and M. J. Padgett, *PNAS* **15**, 3800 (2018).
- [41] J. Courtial, K. Dholakia, D. A. Robertson, L. Allen, and M. J. Padgett, *Phys. Rev. Lett.* **80**, 3217 (1998).
- [42] K. D. Skeldon, C. Wilson, M. Edgar, and M. J. Padgett, *New J. Phys.* **10**, 013018 (2008).
- [43] M. P. J. Lavery, F. C. Speirits, S. M. Barnett, and M. J. Padgett, *Science* **341**, 537 (2018).
- [44] C. Rosales-Guzmán, N. Hermosa, A. Belmonte, and J. P. Torres, *Sci. Rep.* **3**, 2815 (2013).
- [45] D. B. Phillips, M. P. Lee, F. C. Speirits, S. M. Barnett, S. H. Simpson, M. P. J. Lavery, M. J. Padgett, and G. M. Gibson, *Phys. Rev. A* **90**, 011801 (2014).
- [46] S. A. Teukolsky and W. H. Press, *Astrophys. J.* **193**, 443 (1974).
- [47] W. Press and S. Teukolsky, *Nature* **238**, 211 (1972).
- [48] P. Pani, V. Cardoso, L. Gualtieri, E. Berti, and A. Ishibashi, *Phys. Rev. Lett.* **109**, 131102 (2012), arXiv:1209.0465 [gr-qc].
- [49] J. C. Degollado and C. A. R. Herdeiro, *Phys. Rev. D* **89**, 063005 (2014), arXiv:1312.4579 [gr-qc].
- [50] O. J. C. Dias and R. Masachs, *Class. Quant. Grav.* **35**, 184001 (2018), arXiv:1801.10176 [gr-qc].
- [51] S. Hod, *Phys. Rev. D* **88**, 064055 (2013), arXiv:1310.6101 [gr-qc].
- [52] R. Li, J. K. Zhao, and Y. M. Zhang, *Commun. Theor. Phys.* **63**, 569 (2015), arXiv:1404.6309 [gr-qc].
- [53] M. Visser, *Class. Quant. Grav.* **15**, 1767 (1998).
- [54] M. Mironov, *Sov. Phys. Acoust.* **34**, 318 (1988).
- [55] S. W. Hawking, *Nature* **248**, 30 (1974).
- [56] S. W. Hawking, *Commun. math Phys.* **46**, 206 (1976).
- [57] S. W. Hawking, *Phys. Rev. D* **14**, 2460 (1976).
- [58] M. K. Parikh and F. Wilczek, *Phys. Rev. Lett.* **85**, 5042 (2000), arXiv:hep-th/9907001 [hep-th].
- [59] S. Hemming and E. Keski-Vakkuri, *Phys. Rev. D* **64**, 044006 (2001), arXiv:gr-qc/0005115 [gr-qc].
- [60] V. V. Krylov, *Prog. Surf. Sci.* **32**, 39 (1989).
- [61] V. V. Krylov and F. J. B. S. Tilman, *J. Sound Vib.* **274**, 605 (2004).
- [62] V. Denis, A. Pelat, F. Gautier, and B. Elie, *J. Sound Vib.* **333**, 2475 (2014).
- [63] L. Tang and L. Cheng, *J. Sound Vib.* **391**, 116 (2017).
- [64] A. Pelat, F. Gautier, S. C. Conlon, and F. Semperlotti, *J. Sound Vib.* **476**, 115316 (2020).
- [65] F. Cheli and G. Diana, “Introduction to the finite element method,” in *Advanced Dynamics of Mechanical Systems* (Springer International Publishing, Cham, 2015) pp. 311–412.
- [66] O. C. Zienkiewicz, R. L. Taylor, and J. Z. Zhu (2005).
- [67] COMSOL, *COMSOL Multiphysics Modeling Software*.
- [68] A. D. Pierce and R. T. Beyer, *J. Acoust. Soc. Am.* **87**, 1826 (1990).
- [69] M. Visser, *Class. Quant. Grav.* **15**, 1767 (1998), arXiv:gr-qc/9712010 [gr-qc].
- [70] S. W. Rienstra and A. Hirschberg, *An Introduction to Acoustics*.
- [71] M. E. Delany and E. N. Bazley, *Appl. Acoust.* **3**, 105 (1970).
- [72] Y. Miki, *J. Acoust. Soc. Jpn. (E)* **11**, 19 (1990).
- [73] F. P. Mechel, *Formulas of Acoustics.* (2004).